Isı Bilimi ve Tekniği Dergisi, 40, 1, 155-165, 2020
J. of Thermal Science and Technology
©2020 TIBTD Printed in Turkey
ISSN 1300-3615

A COMPARISON OF THE THERMAL PERFORMANCE OF A CONVENTIONAL FIN BLOCK AND PARTIALLY COPPER AND ALUMINUM FOAM EMBEDDED HEAT SINKS

S. Kaancan ATAER*, Cemil YAMALI† and Kahraman ALBAYRAK**
*Space Systems Department, Thermal Control Systems, Turkish Aerospace Inc. (TA), Ankara, Turkey
suleymankaancan.ataer@tai.com.tr
†*posthumous* 13.05.2018
**Mechanical Engineering Department, Faculty of Engineering, Middle East Technical University, Ankara, Turkey
albayrak@metu.edu.tr

(Geliş Tarihi: 02.12.2018, Kabul Tarihi: 05.03.2020)

Abstract: In this research, the metal foams with 4,8,16 pores/cm, an aluminium foam which has 0.93 porosity and a copper foam which has 0.90 porosity that are integrated into a heat sink with a special geometry were designed and tested. During the process of the experiments, the thermal resistances and the pressure losses of the metal foam integrated heat sinks were tested by applying different heat fluxes (10.67, 15.75, 21.33 and 31.50 kW/m^2) and two distinct frontal air velocities (4 and 6 m/s) to the specimens. The differences in the thermal performances of the heat sinks were observed by enforcing the custom-made manufactured heaters. The test results demonstrate that the pressure drop of the foam heat sinks is approximately four times more than the fin block; the average convection heat transfer coefficients of foam heat sinks are not dependent to the heater loads and the base plate temperatures of the foam sections were 1 to 1.5 degree lower than the foamless sections. This heat sink design provides lower temperatures on the desired locations of the electrical components than a conventional type fin block.
Keywords: Copper Foam, aluminum foam, soldering method, forced convection, conduction, thermal management

GELENEKSEL KANATÇIKLI BLOK VE KISMİ ALÜMİNYUM VE BAKIR METAL KÖPÜK YERLEŞTİRİLMİŞ ISI ALICILARIN ISIL PERFORMANSLARININ KARŞILAŞTIRILMASI

Özet: Bu araştırmada, 4,8,16 gözenek/cm oranında 0,93 gözenekliliğe sahip alüminyum ve 0,90 gözenekliliğe sahip bir bakır metal köpükler kullanılarak özel bir geometriye sahip ısı alıcı tasarlanmış ve test edilmiştir. Deneyler sırasında, metal köpük entegre edilerek üretilmiş ısı alıcıların ısıl dirençleri ve basınç kayıpları, farklı ısı akıları (10.67, 15.75, 21.33 ve 31.50 kW / m2) ve iki ayrı ön hava hızı (4 ve 6 m/s) uygulanarak test edilmiştir. Isı alıcıların ısıl performanslarındaki farklılıklar, özel olarak ürettirilen ısıtıcıların kullanılarak gözlenmiştir. Test sonuçları, köpük ısı alıcılarının basınç düşüşünün kanat bloğundan yaklaşık dört kat daha fazla olduğunu göstermektedir; köpük ısı emicilerinin ortalama konveksiyon ısı transfer katsayıları ısıtıcı yüklerine bağlı değildir ve köpük bölümlerinin taban plakası sıcaklıkları, köpüksüz bölümlerden 1 ila 1.5 derece daha düşüktür. Bu ısı alıcı tasarımı, elektrikli cihazların bileşenlerinin istenen konumlarında geleneksel tip bir kanatçıklı bloktan daha düşük sıcaklıklar sağlamıştır.
Anahtar Kelimeler: Bakır Köpük, Alüminyum Köpük, Lehimleme Yöntemi, Zorlanmış Konveksiyon, İletim, Isıl Yönetim

NOMENCLATURE

A_{con}	Convection area of the heat sink $[m^2]$
A_{cs}	Cross section area of a duct $[m^2]$
a	Duct channel width $[m]$
b	Duct channel height $[m]$
D_{HF}	Hydraulic dia. of duct for heat sinks $[m]$
$\bar{h}$	Avg. convection HTC $[\mathrm{W/m^2 \cdot K}]$
I_f	Fan current $[A]$
I_h	Heater current $[A]$
K	Permeability of the porous zones $[m^2]$
k	Thermal conductivity $[\mathrm{W/m \cdot K}]$
l	Length of a fin $[m]$
Nu	Nusselt number
P	Pressure of a fluid [Pa]
PPI	Number of pore per inch
$\dot{Q}$	Heat transfer rate [W]
q	Heat flux [W·m^{-2}]
Re	Reynolds number
R_{th}	Thermal resistance [°C/W]
T_{avgb}	Average base plane temperature [°C]
$T_{c,in}$	Coolant inlet temperature [°C]
$T_{c,out}$	Coolant mean exit temperature [°C]
t	Fin thickness of a fin block [m]
U	Velocity of a fluid [m·s^{-1}]
V_f	Fan voltage [V]

V_h Heater voltage [V]
$\dot{W}$ Pumping power [W]
Δ Change
μ Viscosity of a fluent [$kg \cdot m^{-1} \cdot s^{-1}$]
ν Kinematic viscosity [$m^2 \cdot s^{-1}$]
ρ Density of a fluid [$kg \cdot m^3$]

Subscripts
c Coolant
e Outlet
h Heater
i Inlet

INTRODUCTION

The miniaturization of the electronic components in the form of integrated circuits (ICs), such as microprocessors, resistors, diodes, plastic leaded chip carriers (PLCCs), etc., increase the geometrical complexity of the electronic devices in restricted spaces. Known as Moore's law, it specifically predicts the doubling of the number of transistors on a given die area every two years. This was later updated as 18 months and it has the validity on the latest semiconductor fabrication technologies as well. At the result of this trend, the compact and small structured electronic box designs require custom-designed cooling systems. The general cooling requirements for the electronic devices require internally generated heat to be spread by optimally arranging the heat flow paths from the source to the sink. Otherwise, the heat cannot be removed away from the surface of the component and an uneven temperature distribution profiles, or hotspot(s) occur. To form near-ideal heat flow paths, the thermal design engineers use all of the three modes of the heat transfer; the conduction, the convection and the radiation. The majority of the applications use both the conduction and the convection to cool the electronic assemblies. At this point, the extensive surface areas, the lower density and the convenience utilization, as well as the open cell metal foam (OCMF) become a considerable material for the heat sink applications. Similar researches, including the OCMF utilization as a heat sink, have been summarized and examined as follows.

In the early studies, Kamath et al. (2013) tested the thermal conductivity and the pressure drops of two different thicknesses, which were the 10 and the 20 PPI aluminum and copper foams. There were two distinct properties of this study. One was locating the testing channel of the foams as vertical and the other was not using any permanent joint method. Screws were used to compress the heater between the foams and the insulating wooden boxes that cover the outer surface of the foams. Kamath also calculated the permeability and the drag coefficient by using Hazen-Dupuit-Darcy approach.

Mancin et al. (2012) calculated heat transfer coefficients of 5, 10, 20 and 40 PPI copper foam blocks whose porosities change between 0.905 and 0.934. In this research, they selected 25, 32.5 and 40 kW/m^2 thermal loads with 0.0055 and 0.0125 kg/s air mass flow rates as the testing samples. These test specimens were compared with their mean wall temperatures, pumping power and their interstitial heat transfer coefficient values. Mancin et al. had another study (2010) that evaluated the pressure drop of six distinct pore density aluminum foams during the air flow. The scope of this study was comparing the experimental and the theoretical analysis pressure drops of six samples. Two of Mancin's key researches give extensive data about the metal foam heat sink performance.

Additionally, Dukhan et al. (2005 and 2007) studied thermal performance of 10 PPI and 20 PPI metal foam heat sinks. Both studies measured the temperature from the holes inside of the aluminum foam samples. Researchers provided a model to predict the thermal behaviors of the metal foam heat sinks. The samples were brazed onto the base heating plates to eliminate the contact resistances. A significant difference between the two studies is the directions of the measured temperatures of the samples.

A Turkish researcher, Ateş (2011) compared the thermal and hydrodynamic performances of the microchannel and the aluminum metal foam heat exchangers. In his study, the microchannel heat sinks with four different channel width and the aluminum foam heat sinks with three different pore densities were tested. Some of the aluminum foams were compressed with 2 and 3 compressed factors by using a special jig. The properties of the preferred aluminum foams were 10, 20 and 40 PPI with 92% porosity respectively.

Hernandez (2005) researched the 6101-T6 aluminum foams under three headings: The first one was the fluid flow and the pressure drop, the second was the forced convection and the last one was the thermal management. At the beginning, various porosity and the pore density foams were tested in the air duct. Even though the air velocities were measured from seven different sections of the foams, the pressure values were measured only at the inlet and the outlet of the samples.

Kim Y. (2001) and Calmidi (2000) investigated the convection heat transfer performances of the aluminum foam matrices. In both studies, the changes of the Nusselt numbers with respect to the Reynolds numbers were calculated for all of the aluminum samples. In these studies, Kim S.Y. (2001) tested the convective heat transfer characteristics of the aluminum foam under the asymmetrically heated channel by a hot bath. Calmidi (2000) tested seven distinct aluminum specimens which had various porosity values with three pore densities.

Although Bhattacharya et al. (2002) found and compared the design parameters of the RVC (reticulated vitreous carbon) and the aluminum foam samples in his research, Peak et al. (2000) generated same parameters, the thermal conductivity, permeability and the internal coefficients only for the aluminum foam samples.

The goal of Nawaz et al. (2010) study was the utilization of the 10 PPI aluminum 0.93 porosity foam heat exchangers instead of the conventional aluminum brazed fins. The aluminum foam was joined to the base plane by a polysynthetic thermal compound which had 5 W/m·K for the base plane. This chemical had relatively lower thermal conductivity compared to a Lead-Tin solder paste type joining material (k = 39 W/m·K) (Loh et al. 2000) which is used in this research.

Mahjoob and Vafai (2008) categorized the literature researches about the metal foam heat exchangers into three main parts; the micro structural-based correlations for the metal foam heat exchangers, the metal foam tube heat exchangers and the metal foam channel heat exchangers. The purpose of their study was to obtain Nu, Re and the pressure drop correlations for each category. The main inference of this study is that inserting the metal foam into a tube or a channel considerably increased the performance of the metal foams.

Bonet, Topin and Tadrist (2008) studied the flow in porous media and they tested dozens of foam samples from different metals or alloys (Cu, Ni, Ni-Cr). Air and water are used as a working fluid with two distinct velocity ranges; first from 0 to 20 m/s and then from 0 to 0.1 m/s, respectively. Their main concern was investigating the compressibility and the pore size effects on the flow field. The pressure values of various pore sized metal foams were measured by twelve pressure sensors which were located on the top side of the test section, through the main flow axis.

Dukhan and Ali (2012) examined the porous metal foams to determine the wall and the size effects on the pressure disturbances. Fourteen different cylindrical 6-inch *length metal foam specimens* were tested in this study. Seven of the samples had diameter changes which were from 1.27 cm to 8.89 cm, 10 PPI with 89.27% porosity and 20 PPI 90% porosity samples with the same pore diameters. During the experiments, the air velocity changed from 0 to 30 m/s which were sufficient enough to obtain the effect of diameter on the pressure distribution. After merging the empirical data to the Darcy-Weisbach friction factor (f_σ) equation, the coefficients were calculated.

Liu et al. (2006) practiced an experimental study to examine the flow friction characteristics of the aluminum foams. Seven different porosity samples were used in order to find a correlation between the friction factor (f_k) and the Reynolds number.

Another practical study was done by Kim et al. (2000) which had a difference at the metal utilization compared to the others. Instead of a louvered fin, the rectangular section foams were embedded into the plate fin heat exchanger. While the hot water was being circulated into the copper jackets, the air flowed through the aluminium foams with 20 ℃ inlet temperature. Both the inlet and the outlet air temperatures as well as the entrance and the exit pressures of the air were measured.

Lastly, Antohe et al. (1997) participated in a distinct study that examined the hydraulic characteristics of the nine compressed open-cell aluminum foams. During the study, the specimens were tested by air and Poly-alpha-olefin (PAO) working fluids. Antohe determined the permeability and the inertia coefficients, which were between $1.0\times10^{-10}m^{-2} < K < 12\times10^{-10}m^{-2}$ and $0.3\ m^{-1} < C < 0.9\ m^{-1}$. Authors claimed that by obtaining these parameters from a curve fitting was more correct than using a one data point. According to this study, the dependence between the permeability and the inertia coefficients with the velocity range was observed.

In this study, a foam in the form of a staircase is soldered at two different locations as shown in Figure 1. The staircase foam utilization is totally different from the literature geometries and this structure requires a lower pressure difference with respect to a mono-block structure which was examined in Mancin's studies (2010) and (2012). It was observed that the two distinct foam sections simulate the two adjacent excessively heated hotspots situation, which was a possible scenario for the electronic box or the cold plate designs. The reason for using a second foam section at the downstream side is to observe the heat transfer performance of the metal foams when the high temperature air is forced to spread the heat from the surface of the metal foam. The staircase alignment of the foams increase the amount of the metal in the downstream direction which provides a higher heat capacity. Additionally, the length of the foam (at the Z direction) extends to the end of the heat sink that forces the air to pass through the metal foam. After an extensive literature survey, a design for a metal foam embedded electronic box cooling with respect to industrial concerns was not observed. The main goal of the current heat sink design is to catch an optimum pressure difference, the mass and the thermal performance. In this paper, the manufacturing methods of the heat sinks and the test set up will be defined in detail at the beginning. It will be followed by the heat transfer measurements, the pressure drop calculations and the extensive presentation of the performance comparison of the heat sinks.

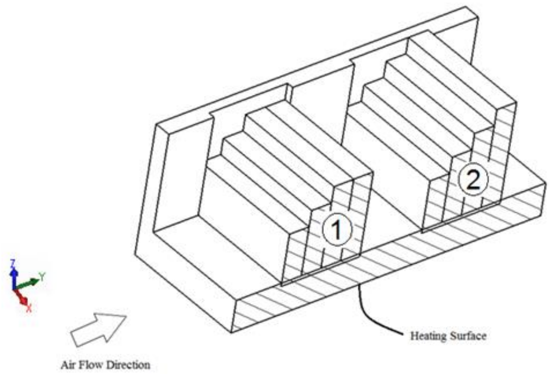

Figure 1. The cross section view of the designed foam embedded heat sink specimens

MANUFACTURING OF THE HEAT SINKS AND THE TEST SPECIMENS

For the current study, a unique heat sink geometry with embedded aluminum and copper foams have been produced. Embedding the foams to aluminum 6061 chassis is achieved by following various steps such as soldering, cutting and coating. An electro discharge cutting process of foams is performed as it is submerged in water.

The thermocouple locations are obtained by a deep-hole drilling process. The machine is used in this step which works like an EDM cutting machine and it has various removable blades. A blade of one millimeter in diameter and thirty millimeters in length are used to drill the heat sink chassis. In this process, the blade caused melting of the aluminum which was then removed from the chassis until the hole reached a depth of thirty millimeters. The six foam chassis and bare fin block were drilled as shown in Figure 2.

Figure 2. The photo of the aluminum fin block heat sink and the thermocouple holes

Both the aluminum foams and their chassis are coated with tin and copper. The reason for the copper coating of all of the foam heat sink chassis is to make them suitable for the soldering operation. A bare aluminum cannot solder itself, so a copper coating is used to create a soldering layer on to the aluminum. After the copper coating operations, all of the foams and their chassis are coated with tin for protection from the effects of corrosion.

Soldering and brazing are the most common joining methods of the metal foams. The most important advantage of these methods is using high thermal conductivity of assistant materials. Both brazing and soldering methods require dissimilar infrastructures. MIKES, a Turkish avionics company, permits usage of its SLC Vapour Phase Soldering Machine for this research. Therefore, soldering methods become applicable for the metal foam joining in extent of this study. The soldering process can be divided in two parts: The Pre-soldering Operations and The Soldering of the Foams to the Chassis of the Specimens in a Vapor Phase Soldering Machine. These are detailed in the following subtitles. The thermal conductivity of the solder, which is composed of 63% tin and 37% lead, is 39 W/m·K (Loh et al. 2000).

The metal foams are inserted into the cream solder that are applied in the pockets of the aluminum chassis which were designed previously. Four different length foams are installed into each pocket. The Lengths of the foams are 16 mm, 21 mm, 26 mm and 31 mm. The SLC 600 Vapor Phase Soldering machine is used for soldering operations of metal foams to the aluminum chassis. This machine commonly solders electrical components on to a bare PCB.

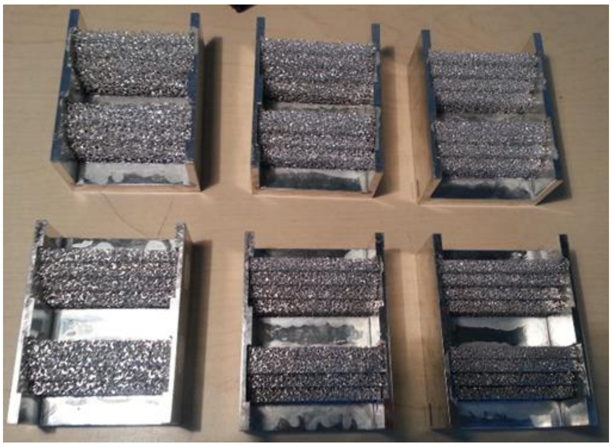

Figure 3. The final form of the soldered metal foam heat sinks

After the soldering operation, the electrical resistivity between the foam and the aluminum chassis is measured with an ohmmeter. The electrical resistivity was measured to be lower than 0.01 mΩ, which means the foams and the chassis behave like a single metal body.

The heat sinks which have identical external dimensions were placed on the testing section of the test rig. The heat sinks are 75 mm wide and 100 mm long with a 10 mm base plate thickness geometries. The aluminum fin block and the external part of the foam-embedded heat sinks were produced from aluminum 6061-T6 alloy. The final forms of the heat sinks are shown in Figure 3.

The external dimensions of the supplied foam plates are 150 mm wide, 150 mm long and 6.35 mm thick. Three particular pore densities were selected for this study through a literature survey. The pore density refers to the number of pores per centimeter or per inch. The pore densities of the samples are 4 pores per cm, 8 pores per cm and 16 pores per cm for both the copper and the aluminum plates. The physical properties of the foam materials are given in Table 1.

Table 1. The physical properties and the geometrical characteristics of the foam plates from literature

Foam	Avg. Pore Dia. (m)	Porosity	Area Density (m^2/m^3)	Area(m^2)
AL 10PPI	0.00508	0.93	809.1	0.058442
AL 20PPI	0.0029	0.93	1240.2	0.089581
AL 40PPI	0.001702	0.93	1800.8	0.130074
CU 10PPI	0.0050	0.905	831.0	0.060024
CU 20PPI	0.00254	0.905	1273.8	0.092006
CU 40PPI	0.00165	0.905	1849.5	0.133595

Each heat sink has 2 pieces which are 16 mm long; 2 pieces which are 21 mm long; 3 pieces which are 26 mm long and 1 piece which is 31mm long. Each part was cut from the same foam plate. The heights of the foam layer heat sinks are shown in Figure 4.

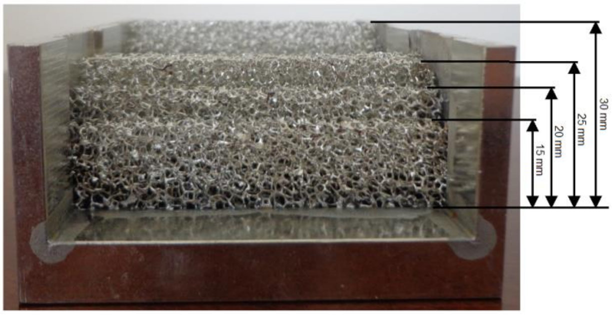

Figure 4. Porous layers of foam embedded heat sink

There are several reasons why the metal foams were used in different heights. The first is to reduce the pressure difference of the heat sink by decreasing the foam thickness. The second is to use the cooling capacity of air efficiently and the last reason is to catch the appropriate heat transfer point between the conduction and the convection heat transfer methods.

TEST SET UP

The primary goal of this experiment was to observe the hydraulic and the thermal behaviour of an aluminium fin block, the open cell copper and the aluminium foam embedded heat sinks. There were fifty-six test cases which were run for seven distinct heat sinks by four separate heaters and two distinct air velocities in total. At the foam embedded heat sinks only the metal foam materials were used to remove the heat from the surface of the heater to the air.

The performance of the heat sinks was evaluated with respect to each other by the inlet and the outlet fluid temperatures, their average base plane temperatures and their pressure drops through the heat sinks. The components of the test rig, their technical properties and the models are shown in Table 2.

The adapter component of the test rig converts the rectangular cross-section exit area of the fan to the cross section area of the test section, so that air can flow through the test specimens. In this study, all the specimens were aimed to be tested under the same conditions such as; the identical air velocities and the thermal loads. The pressure drops of the heat sinks were calculated via the power consumption of the fan.

At the first step of the test rig assembly, item no 5 (see Table 2), the adapter, was attached to the test section (item no 6) with four hexagonal-headed M6 screws by implementing the O-Ring gasket into the hole of test section. Secondly, the honeycombs which prevent the fluctuation of the anemometer AIRFLOW TA2 were placed inside of the adapter.

Following this procedure, in order to install the fan, four hexagonal headed screws and 20 mm long M6 were fastened by pressing the gasket of the adapter part. The subassembly of the test rig was installed to the POM spacers that pressed the insulation materials between the duct assembly and the aluminum plate with fourteen M4 30 mm length screws. Due to the low thermal conductivity, the low thermal expansion co-efficiency and easy machining properties, polyoxymethylene (POM) was ideal to make the test section duct assembly and the adaptor as well as the fan holders and the spacers of the test rig. Despite the low thermal properties of the POM material, negligible heat losses occurred in the experiments.

Two different types of the heater plates were required for two separate heaters. The plates were designed and manufactured by using Pertinax heat-resistant material. The heaters were compressed between the heat plate and the heat sink by six M4 10 millimeter long screws to avoid the thermal resistance. The partial and the whole heaters are illustrated in Figure 5.

Table 2. Component of the test rig

Item No:	Component:	Properties\Function\Measuring Ranges:
1	Fan	AC centrifugal Fan, Max pressure: 330 Pa, Max Vol. rate: 260 m^3/h
2	Heaters	Heater capabilities: 60W, 120W, 80W, 160W
3	Hot Wire Anemometers # 1	Velocity range: 0-15 m/s, Temperature range: 0- 80 ^oC
4	Hot Wire Anemometers # 2	Velocity range: 0-30 m/s, Temperature range: -30- 200 ^oC
5	Adapter	Reduction of air flow area from fan exit to test section inlet.
6	Test Section Duct Assembly	Providing air flow pass through the heat sinks, locating thermocouples
7	Heater Plates	Thermal Conductivity: 0.21 W/m·K, Thermal Exp. Coeff.: 1.6×10^{-4} C^{-1}
8	Fan Holders	Stabilizing fan during the operation.
9	Insulation Material	Thermal Conductivity: 0.032 W/m·K, Insulating test section from Base Plate
10	Base Plate	Combining all set-up components on the same plane
11	Voltmeter of Fan	AC Current range: 0.3 mA - 10 A, AC Voltage range: 30 mV - 1000 V
12	Ammeter of Fan	AC Current range: 2-400 Ampere, AC Voltage range: 2-600 Volt
13	Voltmeter of Heater	AC Current range: 10 mA - 10 A, AC Voltage range: 10 mV - 1000 V
14	Ammeter of Heater	AC Current range: 10 mA - 10 A, AC Voltage range: 10 mV - 1000 V
15	AC Motor Driver	Output: 750 W, Input Voltage: 200VAC, Input Current: 6.5A, Output Current: 3.6A
16	Frequency meter	AC Current range: 0.4 mA - 20 A, AC Voltage range: 1000 mV - 1000 V
17	Thermocouples	Digi-Sense Thermocouple,Wire,TYPE-T,30-GAUGE, FEP Insulation,
18	Power Supply	Superior Electric Powerstat 216B Variable Autotransformer, Input Volt: 240V Output Volt: 0-280V Frequency: 50-60 Hz
19	Data Logger	Up to 120 Channels, 11 function measuring capability, voltage, ampere, and temperature recorder within 1 second's intervals.
20	Laptop	Collecting & Processing data taken from Data logger

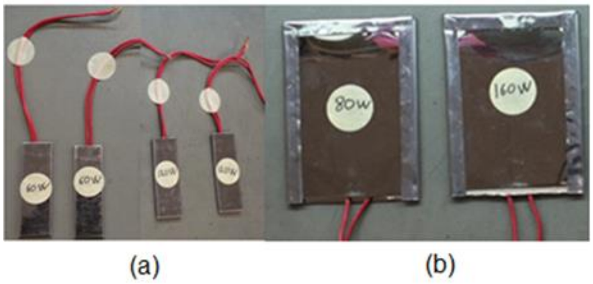

Figure 5. (a) Partial heaters; (b) whole heaters

THE HEAT TRANSFER MEASUREMENTS AND THE PRESSURE DROP CALCULATION

The Pressure Drop

The pressure drops of the test specimens were calculated via the power of the fan as in Equation 1.

$$\Delta P = \frac{\dot{W}}{\dot{Q}} = \frac{Uab}{I_f V_f} \qquad \textbf{(1)}$$

The Reynolds numbers of the fin block which were calculated in Equation 2 proved that the flow was in a laminar regime. The pressure drops, the Reynolds numbers of the fin block and their uncertainties are presented in Table 3. The pressure drops of the fin block were lower than all other kinds of the metal foam heat sinks.

$$Re = \rho u \frac{D_{HF}}{\mu} = \frac{u2lt}{(l+t)\nu} \qquad \textbf{(2)}$$

Table 3. The pressure drops of the fin block

	$\dot{m}$ (kg/h)	ΔP (Pa)	Re
Bare Fin	33	36	957
	50	70	1435

Column 2 of Table 4 shows the pressure drops of the foam embedded heat sinks calculated by using the fan power consumption measurement whereas the column 3 shows the pressure drops of the foams which have the same structure were calculated with Hazen-Dupuit-Darcy Equation (Mancin et al. 2010, 2012).

Table 4. Tabulated pressure drop results

FOAM	$\dot{m}$ (kg/h)	ΔP (Pa)	$\Delta P_{cal.}$ (Pa)	$Re_{cal.}$
AL10PPI	33	80	199.87	131
	50	157	436.93	196
AL20PPI	33	93	256.14	87
	50	208	547.32	130
AL40PPI	33	148	379.35	76
	50	292	815.85	114
CU10PPI	33	71	181.26	105
	50	141	388.08	158
CU20PPI	33	84	244.04	70
	50	189	504.27	105
CU40PPI	33	139	356.53	61
	50	250	743.95	92

As shown in Equation 3, the Reynolds number of the porous media was calculated where the permeability values of the foam samples were taken from Mancin's studies (2012, 2010). Although the porosity and the pore density of the tested metal foams were similar to the Mancin's study, the heat sink geometries cause different pressure drop from those of Mancin's study. As mentioned in the introduction, the manufacturing sections in the current research have a unique heat sink geometry and a lower metal foam than the mono-block structures. Because of the staircase design, air can pass more easily through the thinner metal foam layers compared to the mono-block metal foams.

$$Re = \frac{\rho U \sqrt{K}}{\mu} \qquad \textbf{(3)}$$

For the current study, due to the thickness and the alignment of the foam, the pressure drop values had to be lower than those of Mancin's. The pressure drop data calculated via the power of the fan were approximately 35-40% were lower than Mancin's data (see also Figure 6).

Alvarez’s (2005) study also confirmed the calculated data with a similar experiment. In Alvarez's study, pressures of the same pore density samples were decreased by reducing the thickness. The staircase alignment of the foams reduced the pressure drops of the specimens as demonstrated in Table 4.

The pressure drop variation versus the pore density is shown in Table 4 and Figure 6. It is obvious that the increase of the pore density and the air frontal velocity enhance the pressure drops of the foam heat sinks. It is known that even though the aluminum foam samples have 93% porosity, the copper ones have 90.5% porosity. The effect of this porosity difference is also seen in Table 4. In fact, the higher porosity aluminum heat sinks have higher pressure drop values compared to the copper heat sinks.

The air velocity directly increases the pressure drops and the Reynolds numbers of all the tested specimens. At the Mancin's study, a rectangular box was selected as the geometry of foams. The effect on the pressure drop of the staircase structure of the heat sinks can be seen in Figure 6.

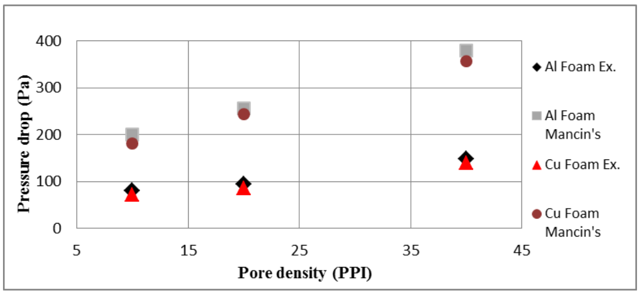

Figure 6. The drop of the tested heat sinks variation and Mancin's results (2012, 2010) with respect to the pore densities

Heat Transfer

In this experiment, the convection coefficients, the Nusselt numbers and the hydraulic diameter of the metal foams were calculated from Equation 4, Equation 5 (Hernández 2005) and Equation 6 (Boomsma, 2002).

$$\bar{h} = \frac{q}{A_{con}(T_{avgb} - T_{c,in})} = \frac{V_h I_h}{A_{con}(T_{avgb} - T_{c,in})} \tag{4}$$

$$Nu = \frac{q D_{HF}}{k_f A_{con}(T_{avgb} - T_{c,in})} = \frac{\rho u c_p 2a^2 b^2 (T_{c,o} - T_{c,i})}{k_f A_{con}(T_{avgb} - T_{c,in})(a+b)} \tag{5}$$

$$D_{HF} = \frac{4A_{cs}}{p} = \frac{4ab}{2(a+b)} \tag{6}$$

$$R_{th} = \frac{\Delta T}{q} = \frac{\Delta T_{avgb} - T_{c,in}}{\dot{m}c(T_{c,out} - T_{c,in})} = \frac{\Delta T_{avgb} - T_{c,in}}{\rho u c a b (T_{c,out} - T_{c,in})} \tag{7}$$

The Nusselt numbers of the fin blocks are calculated with Equation 5 which is shown in Table 5. The Nusselt numbers of the foam embedded heat sinks are higher than the fin block as demonstrated in Table 6 and Table 7. The thermal resistances, Nusselt numbers, the convection coefficients of the tested foam embedded heat sinks are presented in Table 6 and Table 7. While Table 6 shows the results of the foam embedded heat sinks at 4 m/s air inlet velocity, Table 7 shows the results of the foam embedded heat sinks at 6 m/s air inlet velocity. On the one hand, the pore density increases the heat transfer area of the foams and the Nusselt numbers decay with a rising pore density. On the other hand, the increased pore density reduces the thermal resistance of all the heat sinks except for the 20PPI copper foam. Because of the manufacturing defects a specific region of the 20 PPI copper layer, as shown in Figure 7, it does not have a uniform porosity through the whole plate. The reason for this manufacturing defect may be originated from the breaking of the ceramic mold during the investment casting process. Finally, the experimental results show that the thermal resistance of a 40 PPI porous heat sink and a 20 PPI porous one do not go in line with the literature trend, as seen in Table 6 and Table 7.

Table 5. The heat transfer coefficients, Nusselt numbers and the thermal resistances of the fin block for both air velocities 4 m/s and 6 m/s

	Heater (W)	$\dot{m}$ (kg/h)	R_{th} (K /W)	Nu
Bare Fin	60	33	0.346	5.90
	80		0.339	5.41
	120		0.365	5.13
	160		0.337	5.25
	60	50	0.290	6.44
	80		0.242	6.51
	120		0.305	6.33
	160		0.225	6.63

The 60 W and the 120 W heaters have the same width as the foam sections of the heat sinks, which is 23.4 mm(1"). The 80 W and the 160 W heaters have the same 100 mm width as the heat sink. This can be seen in Figure 5. Although this heater size effects the thermal resistance of the fin block as in Table 5, an increasing thermal resistance trend is seen with the increasing heater power at the foam heat sinks in Table 6 and Table 7. The main reason for the higher thermal resistance values at two partial 1" size 60 W and 120 W heaters is the inadequacy in the fin block heat transfer area. The baseplate temperature of the fin blocks is higher than the foam embedded heat sinks in all of the test cases, which shows the heat accumulation at the base plate of the fin block. Foam metals with a superior property in the excessive heat transfer area solves this heat transfer area inadequacy.

The high thermal conductivity of the copper samples ensured the superior thermal performance of the copper foams. The effects of air velocity can appear when the heat transfer coefficients and the thermal resistances of Table 6 are compared to those of Table 7. The 10 PPI copper embedded heat sinks had the highest heat transfer coefficients. The 10 PPI aluminum embedded heat sinks took the second place.

Table 6. The heat transfer coefficients, Nusselt numbers and the thermal resistances of the metal foam embedded heat sinks at 4 m/s air velocity

	Heater (W)	$\dot{m}$ (kg/h)	R_{th} (K /W)	$\bar{h}$ (W/m²·K)	Nu
Al10PPI	60	33	0.290	39.79	62.75
	80	33	0.324	39.94	62.99
	120	33	0.352	38.52	60.75
	160	33	0.324	39.28	61.94
Al20PPI	60	33	0.287	27.35	43.13
	80	33	0.331	26.18	41.29
	120	33	0.333	26.24	41.37
	160	33	0.266	25.81	40.71
Al40PPI	60	33	0.260	18.03	28.44
	80	33	0.261	17.62	27.78
	120	33	0.250	17.30	27.27
	160	33	0.264	17.47	27.55
CU10PPI	60	33	0.273	42.41	66.88
	80	33	0.241	43.86	69.16
	120	33	0.251	42.99	67.80
	160	33	0.319	43.99	69.37
CU20PPI	60	33	0.105	37.08	58.47
	80	33	0.145	32.27	50.88
	120	33	0.138	31.86	50.24
	160	33	0.141	30.92	48.76
CU40PPI	60	33	0.185	24.19	38.14
	80	33	0.196	23.06	36.36
	120	33	0.217	23.44	36.96
	160	33	0.229	23.77	37.48

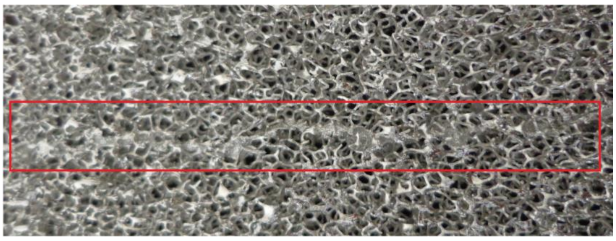

Figure 7. The picture of the closed cells of the copper foam plate

The increase of the pore density impeded the air flow through the metal foam. As a result, the convective heat transfer from the metal foam to air was reduced by the increasing pore density as expected. Finally, it is understood that the thermal resistance is directly dependent on the pore density of the foam samples. All of the thermal resistances, except for the 20PPI copper, were lessened with the pore density. As stated in the results, the Nusselt numbers decline along with the rise of the heat transfer areas falls down. This means that the increase of the pore density increases the conduction heat transfer of the foam metals.

Table 7. The heat transfer coefficients, Nusselt numbers and the thermal resistances of the metal foam embedded heat sinks at 6 m/s air velocity

	Heater (W)	$\dot{m}$ (kg/h)	R_{th} (K /W)	$\bar{h}$ (W/m^2·K)	Nu
Al10PPI	60	50	0.207	49.50	78.06
	80	50	0.219	59.13	93.24
	120	50	0.237	49.69	78.36
	160	50	0.207	53.40	84.21
Al20PPI	60	50	0.182	34.72	54.75
	80	50	0.207	34.14	53.83
	120	50	0.220	34.75	54.80
	160	50	0.189	34.56	54.50
Al40PPI	60	50	0.170	22.39	35.31
	80	50	0.220	22.34	35.23
	120	50	0.214	22.39	35.31
	160	50	0.191	22.57	35.58
CU10PPI	60	50	0.178	53.68	84.64
	80	50	0.205	56.21	88.64
	120	50	0.236	55.37	87.32
	160	50	0.203	56.56	89.19
CU20PPI	60	50	0.074	42.02	66.26
	80	50	0.086	42.71	67.35
	120	50	0.084	41.15	64.89
	160	50	0.134	41.48	65.41
CU40PPI	60	50	0.119	31.90	50.30
	80	50	0.171	33.60	52.99
	120	50	0.151	32.18	50.75
	160	50	0.152	31.66	49.92

Figure 8 and Figure 9 show the thermocouple temperatures of the base plane at the stated conditions. Due to the locations of the heaters, the temperatures on the foam sides were higher than TC9 and TC5 in Figure 8. In addition, the metal foam parts in Figure 9 provided the temperature values which get close to one another. The heat transfer coefficients (HTC) of each sample showed similar values at various heaters as mentioned in Mancin's study (2012). In addition, the order of the heat transfer coefficients with respect to the pore density of the present study and Mancin's study support one another (2012). Another study carried out by Mancin indicated that the 10 PPI aluminum sample had lower mean wall temperature than the 20PPI and the 40 PPI foams which are at the same porosity, as in Figure 10.

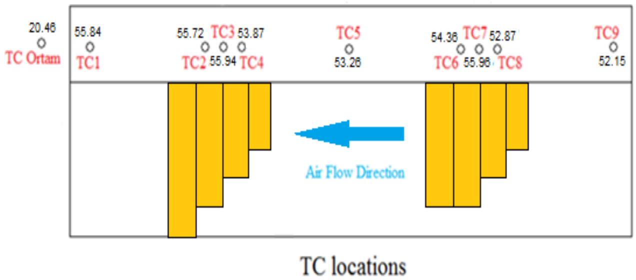

Figure 8. Surface temperatures of CU 20PPI at a 2 section 120 watt heater at 6 m/s air velocity

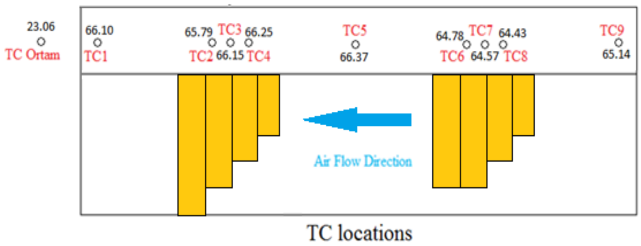

Figure 9. Surface temperatures of CU 20PPI at a whole 160 watt heater at 6 m/s air velocity

At the copper samples, the increase of the pore density decreases the mean wall temperature of the heat sinks as seen in Figure 10. On the contrary, the mean wall temperatures of the aluminum heat sinks increase with pore density. This can be interpreted as, the higher porosity and the lower thermal conductivity of the aluminum foams slowed the heat flow from the foam surface to air.

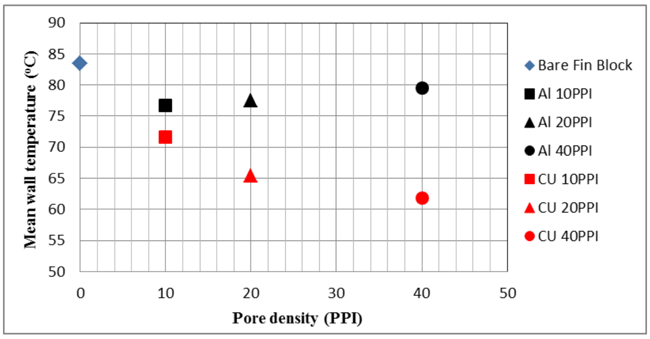

Figure 10. Mean wall temperature as a function of pore density at 160 W heater and 6 m/s frontal air velocity

THE PERFORMANCE COMPARISON OF THE HEAT SINKS

This study has one ultimate goal which is to determine the heat sink that will give the lowest base temperature at a specified heater load and the inlet air temperature with the lowest air pressure drop. Figures 13 was prepared for the evaluation of the heat sinks with the best performance heat sinks for this goal. The thermal resistances of the heat sinks were calculated by implementing Equation 7.

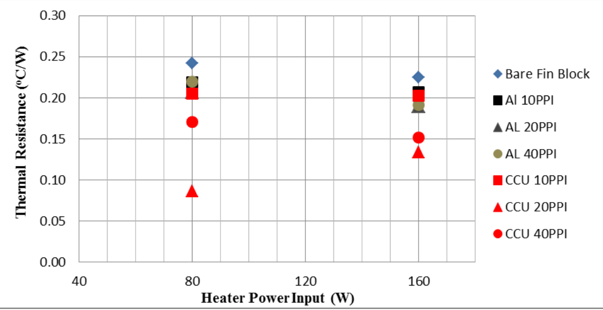

Figure 11. Variation of R_{th} as a function of heater power at 50 kg/h mass flow rate (whole heaters)

As it can be seen in Figure 11, the thermal resistances of the heat sinks drop down at 160 W heater loads. There could be a breakeven point beyond which heat sink works effectively. The effectiveness of the heat sink depends on the heater load and the geometrical configuration of the heat sink, which seems to be worth investigating in further studies. The 20PPI foam embedded heat sinks do not fit in this generalization. The reason for this discrepancy can be originated from the closed cell structure of the copper foam plates. It is clearly understood from the Figure 11 that the fin block has the highest thermal resistances at both heat loads. While the thermal resistances of the aluminium foams are close to each other, the thermal resistances of the copper foams illustrate the differences. The effect of the thermal conductivity of the copper samples is seen in the 20PPI and the 40PPI copper foam embedded heat sinks which have the lowest thermal resistances.

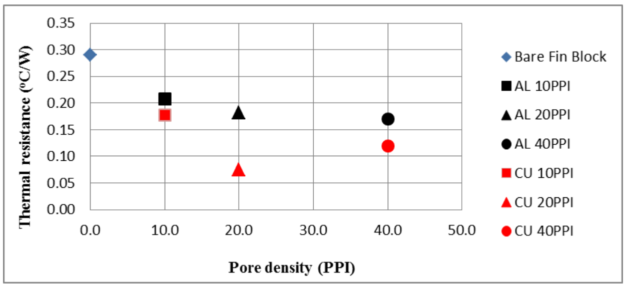

Figure 12. Variation of R_{th} as a function of the pore density at a 60W heater and 6 m/s frontal air velocity

It is observed that the increase of the pore density decreases the thermal resistance of the heat sinks except for the 20 PPI copper sample as seen in Figure 12. Even with the limited usage of the metal foam, the thermal resistance of the metal foam embedded heat sinks are significantly lower than the thermal resistance of the fin block as shown in Figure 12.

Figure 13 demonstrates the base plane temperatures of the samples and the vertical lines indicate the foam boundaries of the heat sinks. It is seen that the temperatures increased in the first foam section while the fresh air provided from a 5 mm gap decreased the second foam section. At the fin block, the temperature continued to increase, which is undesired for the operational life of the electronic components. Finally, the 40PPI copper foam heat sink provided the lowest base plane temperatures. However, the 20PPI copper foam heat sink was the most effective considering the pressure drop and the thermal resistance together. Moreover, the 20PPI foam heat sink produced less noise compared to the 40PPI foam heat sink. The metal foam-structured heat exchangers reduced the thermal resistance by nearly two thirds when compared to a conventional fin block.

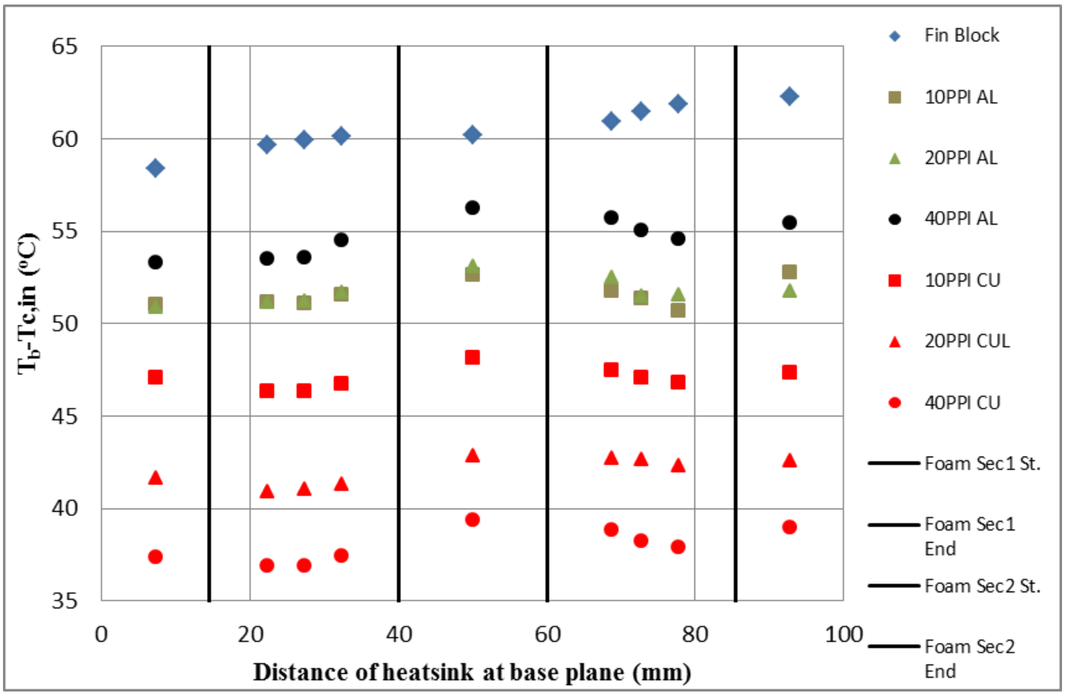

Figure 13. The variation of the base plane temperatures as a function of the distance at 160 W heater

CONCLUSIONS

In this study, an experimental comparison between the thermal and the hydrodynamic characteristics of the partial metal foam embedded heat sinks and those of conventional fin block was presented. The current study not only shows the metal foam embedded heat sink design for the electronic boxes, but also guides the utilization of the metal foams at the industrial heat sinks. The main findings of this study is summarized as follows:

- Both the copper and the aluminum metal foam embedded heat sinks have lower thermal resistance than the aluminum fin block at all heater loads and air velocities. Both the 40 PPI and the 20 PPI copper foam embedded heat sinks are shown convenient to the electronic cooling applications.

- The measured pressure drop of the foam heat sinks increased up to four times more than that of the fin block at 50 kg/h air flow rate, as shown in Table 3 and Table 4. Not only the thermal resistance, but also the pressure difference of the 10 PPI aluminum foam embedded heat sink make it a suitable option among the other aluminum ones.

- The thermal resistance of the foam embedded heat sinks decreased with the increasing pore density as found in the Mancin's study. Only the resistance of the 20 PPI copper foam embedded heat sinks does not fit this trend, which was described under the 'Heat Transfer' subsection. The reasons why Mancin's studies are the guideline researches for the current study are the same pore density foam specimens and the use of the same working fluid.

- At the 80 W and the 160 W larger heater scenarios, the temperature at the foam sections are as low as 1 to 1.5 degree, which is lower than the temperature at the foamless sections. It is clearly observed that locating the metal foam under the equipment that may generate hotspots and it has positive results in terms of equipment performance.

ACKNOWLEDGMENTS

This study was supported by M. Koç, Z.A. Temel, A.H. Erbay, K. Yıldız, M. Kahya, M. Yalçın, S. Gürel and G. Doğan. The authors would like to thank for having a fruitful discussion with Y. Demirtola and A. Ünal. This research did not receive any specific grant from funding agencies in the public, commercial, or not-for-profit sectors.

REFERENCES

Antohe B. V., Lage J. L., Price D. C., Weber R. M., 1997, Experimental Determination of Permeability and Inertia Coefficients of Mechanically Compressed Aluminium Porous Matrices, *Journal of Fluids Engineering,* 119, 404-412.

ATEŞ A. M., 2011, Experimental Comparison of Fluid and Thermal Characteristics of Microchannel and Metal Foam Heat Sinks, *Msc. Thesis, METU.*

Bhattacharya A., Calmidi V.V., Mahajan R.L., 2002, Thermophysical Properties of High Porosity Metal Foams, *International Journal of Heat and Mass Transfer,* 45, 1017-1031.

Bonnet J.P., Topin F., Tadrist L., 2008, Flow Laws in Metal Foams: Compressibility and Pore Size Effects, *Transport in Porous Media*, 73, 233-254.

Boomsma K.S., 2002, Metal Foams as Novel Compact High Performance Heat Exchangers for the Cooling of Electronics, *PhD. Thesis, Swiss Federal Institute of Technology Zurich.*

Calmidi V. V., Mahajan R. L., 2000, Forced Convection in High Porosity Metal Foams, *ASME Journal of Heat Transfer,* 122, 557-565.

Dukhan N., Ali M., 2012, Strong Wall and Transverse Size Effects on Pressure Drop of Flow through Open-Cell Metal Foam, *International Journal of Thermal Sciences,* 57, 85–91.

Dukhan N., Chen K. C., 2007, Heat Transfer Measurements in Metal Foam Subjected to Constant Heat Flux, *Experimental Thermal and Fluid Science,* 32, 624–631.

Dukhan N., Quinones-Ramos P. D., Cruz-Ruiz E., Velez-Reyes M., Scott E. P., 2005, One-Dimensional Heat Transfer Analysis in Open-Cell 10-PPI Metal Foam, *International Journal of Heat and Mass Transfer*, 48, 5112–5120.

Hernández Á. R. Á., 2005, Combined Flow and Heat Transfer Characterization of Open Cell Aluminium Foams, MSc. *Thesis, University of Puerto Rico.*

Kim S.Y., Kang B.H., Kim J.H., 2001, Forced Convection from Aluminium Foam Materials in an Asymmetrically Heated Channel, *International Journal of Heat and Mass Transfer,* 44, 1451–1454.

Kim S.Y., Peak J.W., Kang B.H., 2000, Flow and Heat Transfer Correlations for Porous Fin in a Plate-Fin Heat Exchanger, *ASME Journal of Heat Transfer*, 122, 572-578.

Liu J.F., Wu W.T., Chiu W.C., Hsieh W.H., 2006, Measurement and Correlation of Friction Characteristics of Flow through Foam Matrixes, *Experimental Thermal and Fluid Science,* 30, 329–336.

Loh C.K., Chou Bor-Bin, Nelson Dan and Chou D.J., 2000, Study of Thermal Characteristics on Solder and Adhesive Bonded Folded Fin Heat Sink, *The Seventh Intersociety Conference,* 2, 1-7.

Mahjoob S., Vafai K., 2008, A Synthesis of Fluid and Thermal Transport Models for Metal Foam Heat Exchangers, *International Journal of Heat and Mass Transfer,* 51, 3701–3711.

Mancin S., Zilio C., Cavallini A., Rosetto L., 2010, Pressure Drop During Air Flow in Aluminium Foams, *International Journal of Heat and Mass Transfer,* 53, 3121–3130.

Nawaz K., Bock J., Dai Z., Jacobi A.M., 2010, Experimental Studies to Evaluate the Use of Metal Foams in Highly Compact Air-Cooling Heat Exchangers, *International Refrigeration and Air Conditioning Conference,* 1-11.

Paek J. W., Kang B. H., Kim S. Y., Hyun J. M., 2000, Effective Thermal Conductivity and Permeability of Aluminium Foam Materials, *International Journal of Thermophysics,* 21, 2, 453-464.

Pradeep M. Kamath, C. Balaji, S.P. Venkateshan, 2013, Convection Heat Transfer from Aluminium and Copper Foams in a Vertical Channel - an Experimental Study, *International Journal of Thermal Sciences,* 64 1-10.

Simone Mancin, Claudio Zilio, Andrea Diani, Luisa Rossetto, 2012, Experimental Air Heat Transfer and Pressure Drop through Copper Foams, *Experimental Thermal and Fluid Science*, 36, 224-232.

Süleyman Kaancan ATAER graduated from Mechanical Engineering Department of Gazi University in 2007. Initially, he started his career at MIKES Inc. from September 2010 to March 2014. Secondly, he worked for STM Inc. as a System Engineer for one year. Finally, he has been working as a Space Systems Thermal Design Engineer in Turkish Aerospace Industry, Inc. He received his MSc degree in the year 2014 from the Mechanical Engineering (M.E.) Department of Middle East Technical University. His research interests are Spacecraft Thermal Control and Design, Thermal Mathematical Model Development and Correlation, Space Systems Environmental Testing.

Cemil YAMALI graduated from Mechanical Engineering Department of Middle East Technical University (Ankara, Turkey) in the year 1973. Then, he received his MSc. degree from the same university and his PhD degree from the University of Michigan in 1983. He worked as an Assoc. Prof at METU from 1988 to 2017. His principle research interests were heat transfer, thermodynamics and solar energy.

Kahraman ALBAYRAK graduated from Mechanical Engineering Department of Middle East Technical University (Ankara, Turkey) in the year 1971. He received his MSc. and PhD. degrees from the same department in the years 1974 and 1984, respectively. His research interests are Fluid Mechanics, Fluid Machinery, Boundary Layer, HVAC Systems and Thermo-Fluid Science. He has been supervisor in 38 MSc, 3 PhD researches and has approximately 60 national and international publications. He is currently working for the Mechanical Engineering Department of Middle East Technical University as a lecturer**.**